Journal of Solid State Chemistry 181 (2008) 1983–1991

Contents lists available at ScienceDirect

Journal of Solid State Chemistry

journal homepage: www.elsevier.com/locate/jssc

Synthesis, chemical bonding and physical properties of RERhB$_4$ (RE = Y, Dy–Lu)

I. Veremchuk [a], T. Mori [a,b], Yu. Prots [a], W. Schnelle [a], A. Leithe-Jasper [a], M. Kohout [a], Yu. Grin [a,*]

[a] Max-Planck-Institut für Chemische Physik fester Stoffe, Nöthnitzer Str. 40, 01187 Dresden, Germany
[b] National Institute for Materials Science, Namiki 1-1, Tsukuba 305-0044, Japan

ARTICLE INFO

Article history:
Received 26 February 2008
Received in revised form
8 April 2008
Accepted 20 April 2008
Available online 4 May 2008

Keywords:
YCrB$_4$ structure type
Crystal structure
Magnetic susceptibility
X-ray absorption spectroscopy
Electron localizability indicator
Quantum chemical theory of atoms
(QTAIM)

ABSTRACT

The compounds of rare-earth metals with rhodium and boron RERhB$_4$ (RE = Y, Dy–Lu) crystallize with the orthorhombic structure type YCrB$_4$ (space group *Pbam*, Pearson symbol *oP*24). The crystal structures of the compounds with RE = Y, Er, Tm and Yb were refined by using single-crystal diffraction data. Analysis of chemical bonding for YRhB$_4$ and YbRhB$_4$ was performed by electron localizability indicator and by calculation of quantum chemical charges (quantum theory of atoms in molecules). Boron and rhodium form the 3-D polyanion containing planar nets of three-bonded boron atoms interconnected by rhodium along [001]. The interaction of the RE species with the rhodium–boron polyanion is predominantly ionic. Magnetic susceptibility data of TmRhB$_4$ and YbRhB$_4$ showed that the RE species are in $4f^{12}$ (Tm) and $4f^{13}$ (Yb) electronic states, respectively. In the low-temperature region, the specific heat revealed a Schottky anomaly for TmRhB$_4$ while an antiferromagnetic transition is observed at 3.5 K for YbRhB$_4$. X-ray absorption measurement at the Yb L_{III} edge for YbRhB$_4$ reveals the $4f^{13}$ state of ytterbium.

1. Introduction

Compounds with the stoichiometry 1:1:4 are widely represented among ternary borides in the systems RE–M–B (RE = Sc, Y, rare-earth metals, M = Al, transition metals) [1–7]. A large number of them adopt an orthorhombic YCrB$_4$ structure type [1,3–7]. For rhodium compounds only the existence of YRhB$_4$ and ErRhB$_4$ has been reported. Whereas for the erbium compound the YCrB$_4$ structure type was assigned on the basis of powder diffraction data and corresponding lattice parameters [8], for YRhB$_4$ only the composition was assumed during the phase analysis of the corresponding ternary system [9].

The rare-earth compounds REMB$_4$ represent interesting objects for studies of *f*-electron magnetism [10,11]. Recently, such investigations were performed on REAlB$_4$ single crystals with the heavy rare earths RE = Tm, Yb, and Lu [12–14]. TmAlB$_4$ (YCrB$_4$ structure type) was found to exhibit multiple magnetic transitions below its Néel temperature T_N [15]. Intrinsic building defects were revealed to exist in the crystals [14] due to the presence of fragments of the closely related ThMoB$_4$ structure motif (space group *Cmmm*). Both structure types have similarities due to the presence of a planar boron network with condensed pentagonal and heptagonal rings [13]. Small aluminum and large rare-earth atoms are sandwiched between the boron pentagons and heptagons of adjacent planar nets, respectively. The structure types of YCrB$_4$ and ThMoB$_4$ differ by the arrangement of pentagonal and heptagonal rings. The existence of intrinsic building defects influences the physical properties and is the origin of the anomalous magnetic properties which are observed in TmAlB$_4$ [14].

In view of these structural and magnetic peculiarities we have synthesized and investigated the crystal structure and physical properties of RERhB$_4$ with RE = Y, Dy–Lu.

2. Experimental

2.1. Sample preparation

Rare-earth metal filings (Ames, 99.95%), Rh powder (Chempur, 100 mesh, 99.95%) and crystalline boron powder (Chempur, <100 μm, 99.995%) in stoichiometric amounts were pressed into pellets. The samples with Tm and Yb were sintered in welded Ta tubes. The primary reaction was performed at 800 °C during 3–4 days, and the homogenization annealing was carried out at 1100 °C for 4–6 days. The samples with RE = Y, Dy, Ho, Er, Lu were remelted several times in an arc furnace under argon atmosphere (mass losses 1–3%). Each sample was wrapped in Mo foil and the

* Corresponding author.
E-mail address: grin@cpfs.mpg.de (Yu. Grin).

0022-4596/$ - see front matter © 2008 Elsevier Inc. All rights reserved.
doi:10.1016/j.jssc.2008.04.028

homogenization annealing was carried out at 1100 °C for 4 days in evacuated quartz tubes. All samples were quenched in cold water after homogenization. The whole preparation and sample handling was performed inside an argon-filled glove box ($p(O_2/H_2O) \leqslant 1$ ppm) due to sensitivity of rare-earth metals to air and moisture.

2.2. Crystals growth

The as-cast samples were crushed, ground down and again pressed into pellets, put into pyrolitic-BN crucibles, sealed into Ta tubes, and then heated in a high-frequency furnace at 1550 °C for 25–30 min, slowly cooled to 1300 °C within 2.5–3 h, kept there for 15 min, slowly cooled to 1100 °C within 2.5–3 h, and then quenched to room temperature. The size and quality of the obtained crystals were suitable for X-ray diffraction experiments.

2.3. X-ray powder diffraction

All samples were characterized by X-ray powder diffraction performed with a HUBER G670 imaging plate Guinier camera equipped with a Ge monochromator (Cu$K\alpha_1$ radiation, $\lambda = 1.54056$ Å). Phase analysis was performed using the WinXPOW program package [16]. The lattice parameters were refined by least-squares fitting of powder data with LaB_6 as internal standard ($a = 4.15692$ Å).

2.4. Single-crystal X-ray diffraction

Irregularly shaped crystals of *RE*RhB_4 (*RE* = Y, Er, Tm, Yb) were isolated from samples treated by growth procedure. Their quality was proven by Laue photographs. The single-crystal diffraction intensity data were collected on a Rigaku AFC7 diffractometer equipped with a Mercury CCD detector applying Mo$K\alpha$ radiation ($\lambda = 0.71073$ Å). The structure refinement was performed employing WinCSD software [17].

2.5. Magnetization measurements

Magnetic susceptibility of annealed samples was measured with an MPMS SQUID magnetometer (Quantum Design) in external magnetic fields up to 7 T.

2.6. Specific heat measurements

Heat capacity was measured with a PPMS (Quantum Design) using a transient heat pulse method. The samples were attached to a sapphire sample holder using Apiezon N grease.

2.7. X-ray absorption spectroscopy (XAS)

To obtain further information on the valence of ytterbium species in $YbRhB_4$, X-ray absorption spectra at the Yb L_{III} edge were measured at the synchrotron beamline E4 at HASYLAB at DESY in Hamburg. X-rays were monochromized by a Si (111) double crystal. Obtained spectra were compared with those recorded from reference material Yb_2O_3.

2.8. Calculation procedures

The band structure and electronic density of states were calculated for $YRhB_4$ and $YbRhB_4$ using the density functional theory (DFT) within a local-density approximation (LDA) with the Barth–Hedin exchange potential [18]. The yttrium compound was chosen in order to avoid known difficulties in description of the 4*f* states by LDA. The ytterbium compound was studied because of the $4f^{13}$ state for Yb atoms found by XAS investigation. Within the program package TB-LMTO-ASA [19] the radial scalar-relativistic Dirac equation was solved to get the partial waves. The calculation within the atomic sphere approximation (ASA) includes corrections for the neglect of interstitial regions and partial waves of higher order [20], and an addition of empty spheres was not necessary. The following radii of the atomic spheres were applied for the calculations: $r(Y) = 1.867$ Å, $r(Rh) = 1.551$ Å, $r(B1) = 1.022$ Å, $r(B2) = 0.998$ Å, $r(B3) = 1.005$ Å, $r(B4) = 1.036$ Å for $YRhB_4$ and $r(Yb) = 1.851$ Å, $r(Rh) = 1.555$ Å, $r(B1) = 1.017$ Å, $r(B2) = 0.998$ Å, $r(B3) = 0.997$ Å, $r(B4) = 1.028$ Å for $YbRhB_4$. Basis sets containing Yb(6*s*,5*d*,4*f*) or Y(5*s*,4*d*), Rh(5*s*,5*p*,4*d*), and B(2*s*,2*p*) orbitals were employed for a self-consistent calculation with Yb(6*p*) or Y(5*p*,4*f*), Rh(4*f*) and B(3*d*) functions being downfolded.

The electron localizability indicator (ELI-D,*Y*) for $YRhB_4$ and $YbRhB_4$ was evaluated according to Kohout [21] with a module implemented within the TB-LMTO-ASA program package [19]. The topology of ELI-D was analyzed using the program Basin [22] with consecutive integration of the electron density in basins, which are bound by zero-flux surfaces in the ELI-D gradient field. This procedure, similar to the one proposed by Bader for the electron density [23], allows to assign an electron count for each basin, revealing the additional information about the chemical bonding. The analysis of the electron density and evaluation of the charges for quantum chemical (quantum theory of atoms in molecules (QTAIM)) atoms were performed also with the program Basin.

The orbital decomposition diagrams of ELI-D [24] for Y and Rh were computed using the wavefunctions (for spherically averaged ensemble densities) of Clementi and Roetti [25]. For the Yb atom a relativistic ZORA calculation was performed with the ADF code using the TZ2P basis set [26].

3. Results and discussion

3.1. Crystal structure

The investigated compounds *RE*RhB_4 crystallize with $YCrB_4$ structure type (space group *Pbam*, Pearson symbol *oP*24). The lattice parameters obtained from powder X-ray diffraction data are presented in Table 1. The existence of the previously reported borides $YRhB_4$ [9] and $ErRhB_4$ [8] was confirmed. Five isotypic compounds with *RE* = Dy, Ho, Tm, Yb, Lu were prepared for the first time. The crystal structures of *RE*RhB_4 (*RE* = Y, Er, Tm, Yb) borides were refined from single-crystal X-ray diffraction data (Table 2). Final atomic coordinates and atomic displacement parameters are listed in Tables 3 and 4.

The unit cell volumes of the investigated compounds follow the size of the corresponding rare-earth cations (Fig. 1). A smooth decrease of the volume with increase of atomic number of *RE*

Table 1
Lattice parameters of *RE*RhB_4 compounds (space group *Pbam*, X-ray powder diffraction data, $\lambda(CuK\alpha_1) = 1.54056$ Å, LaB_6 standard)

RE	*a* (Å)	*b* (Å)	*c* (Å)	*V* (Å^3)
Y	5.9553(2)	11.5494(4)	3.5548(2)	244.50(3)
Dy	5.9554(4)	11.5525(7)	3.5492(3)	244.18(5)
Ho	5.9446(2)	11.5292(4)	3.5405(2)	242.65(3)
Er	5.9356(6)	11.5061(6)	3.5286(2)	240.99(4)
Tm	5.9237(2)	11.4843(4)	3.5218(2)	239.59(3)
Yb	5.9187(3)	11.4805(6)	3.5099(2)	238.49(4)
Lu	5.9074(3)	11.4523(6)	3.5080(2)	237.33(4)

Table 2
Data collection and crystal structure refinement of *RE*RhB_4 compounds (space group *Pbam*)[a]

Composition	$YRhB_4$	$ErRhB_4$	$TmRhB_4$	$YbRhB_4$
Z	4			
Diffractometer	Rigaku AFC 7, mercury CCD detector			
Radiation and wavelength	MoKα, $\lambda = 0.71073$ Å			
2ϑ (max)	62.4	63.4	62.4	65.9
Index ranges	$-7 \leqslant h \leqslant 8$ $-16 \leqslant k \leqslant 16$ $-5 \leqslant l \leqslant 3$	$-8 \leqslant h \leqslant 8$ $-15 \leqslant k \leqslant 14$ $-5 \leqslant l \leqslant 3$	$-7 \leqslant h \leqslant 7$ $-8 \leqslant k \leqslant 15$ $-5 \leqslant l \leqslant 5$	$-9 \leqslant h \leqslant 7$ $-17 \leqslant k \leqslant 17$ $-5 \leqslant l \leqslant 4$
Reflections collected	1948	2537	1844	2300
Unique reflections	418	413	389	476
R_{int}	0.024	0.038	0.026	0.038
Observed reflections (with $F_{hkl} > 4\sigma(F)$)	390	396	373	467
Number of free parameters	26			
Mode of refinement	$F(hkl)$			
Extinction coefficient[b]	0.009(1)	0.041(1)	0.017(1)	0.032(1)
Final residuals[c]				
$R(F)_{gt}$	0.031	0.030	0.025	0.036
$wR(F^2)_{gt}$	0.033	0.031	0.026	0.037

[a] For lattice parameters see Table 1. Further details on the crystal structure investigations can be obtained from Fachinformationzentrum Karlsruhe, D-76344 Eggenstein-Leopoldshafen, fax: (+49)7247-808-666: e-mail: crysdata@fiz.karlsruhe.de, on quoting the depository numbers CSD 419358 ($YRhB_4$), CSD 419359 ($ErRhB_4$), CSD 419360 ($TmRhB_4$) and CSD 419361 ($YbRhB_4$).

[b] Extinction formalism: $k[1+0.001xF_c^2\lambda^3/\sin(2\theta)]^{-1/4}$, x — extinction parameter, k — overall scale factor.

[c] $R(F)_{gt} = \sum||F_o|-|F_c||/\sum|F_o|$ $wR(F^2)_{gt} = [w\{|F_o|-|F_c|\}^2/\sum w|F_o|^2]^{1/2}$.

Table 3
Atomic coordinates and displacement parameters for *RE*RhB_4 compounds

Atom	Site		$YRhB_4$		$ErRhB_4$		$TmRhB_4$		$YbRhB_4$	
			x, y	$B_{iso/eq}$[a]	x, y	$B_{iso/eq}$	x, y	$B_{iso/eq}$	x, y	$B_{iso/eq}$
RE	4*g*	$x\ y\ 0$	0.36873(8) 0.14899(4)	0.33(1)	0.36849(4) 0.14896(3)	0.358(9)	0.36866(4) 0.14886(2)	0.277(7)	0.36840(6) 0.14892(3)	0.35(1)
Rh	4*g*	$x\ y\ 0$	0.85843(6) 0.09396(3)	0.339(9)	0.85822(8) 0.09397(5)	0.32(1)	0.85796(7) 0.09435(4)	0.28(1)	0.85776(1) 0.09436(5)	0.36(1)
B1	4*h*	$x\ y\ \frac{1}{2}$	0.0213(9) 0.1925(5)	0.51(8)	0.0230(12) 0.1921(7)	0.40(13)	0.0217(11) 0.1932(6)	0.36(9)	0.022(2) 0.1931(7)	0.4(1)
B2	4*h*	$x\ y\ \frac{1}{2}$	0.1128(10) 0.0474(4)	0.44(7)	0.1141(12) 0.0468(7)	0.54(13)	0.1124(11) 0.0477(6)	0.41(9)	0.1131(15) 0.0472(7)	0.4(1)
B3	4*h*	$x\ y\ \frac{1}{2}$	0.6374(9) 0.0307(4)	0.47(7)	0.6364(12) 0.0314(7)	0.52(14)	0.6355(10) 0.0306(6)	0.37(9)	0.6357(14) 0.0300(8)	0.4(1)
B4	4*h*	$x\ y\ \frac{1}{2}$	0.7092(9) 0.1869(4)	0.41(7)	0.7098(12) 0.1861(7)	0.37(13)	0.7101(12) 0.1875(6)	0.44(9)	0.707(2) 0.1869(8)	0.6(1)

[a] $B_{eq} = \frac{1}{3}[B_{11}(a^*)^2a^2 + \cdots + B_{23}(b^*)(c^*)bc\cos\alpha]$ for *RE* and Rh positions, B_{iso} for boron positions.

Table 4
Anisotropic displacement parameters (Å^2) for *RE*RhB_4 compounds[a]

Compound	$YRhB_4$		$ErRhB_4$		$TmRhB_4$		$YbRhB_4$	
Atom	Y	Rh	Er	Rh	Tm	Rh	Yb	Rh
B_{11}	0.48(2)	0.48(2)	0.26(1)	0.25(2)	0.39(1)	0.40(2)	0.29(2)	0.28(2)
B_{22}	0.27(2)	0.23(1)	0.59(2)	0.61(2)	0.09(1)	0.09(2)	0.40(2)	0.39(2)
B_{33}	0.26(2)	0.31(2)	0.23(2)	0.11(2)	0.35(1)	0.35(2)	0.37(3)	0.39(2)
B_{12}	−0.04(1)	0.01(1)	−0.03(1)	0.02(1)	−0.01(1)	0.02(1)	−0.02(1)	0.03(1)

[a] $B_{13} = B_{23} = 0$.

suggests the same (i.e. trivalent) state for *RE* metals in the present *RE*RhB_4 phases.

The particular characteristics of the crystal structure of *RE*RhB_4 are discussed on the example of $YbRhB_4$. The boron atoms at $z = 1/2$ form planar nets composed of condensed pentagons and heptagons. The adjacent five- and seven-membered rings sandwich smaller rhodium and larger ytterbium atoms, respectively, located at $x = 0$. The coordination of Rh and Yb atoms can be described as pentagonal and heptagonal prisms with the additional metal atoms in front of each side face. Each boron atom centers a trigonal prism formed by metal atoms. The rectangular faces of this prism are capped by three additional boron atoms (Fig. 2a).

The arrangement of the boron atoms in the $YCrB_4$ structure type is closely related to that of boron and carbon atoms found in the ScB_2C_2 type (space group *Pbam*) [27]. In this crystal structure, the positions between the five-member rings (formed by boron and carbon atoms) are empty (Fig. 2b). The $YCrB_4$ type is also related to the AlB_2 type (space group *P*6/*mmm*) with six-membered rings in the boron substructure. The substitution of Al atoms by larger metals (Y, Cr) causes the disproportionation of six-member rings into five- and seven-member rings.

Three structure types with a *REM*B_4 composition are known for ternary rare-earth transition metal borides: $YCrB_4$ (space group *Pbam*) [4], $ThMoB_4$ (space group *Cmmm*) [28] and $ErNiB_4$ (space group *I*4/*mmm*) [29] (Table 5). While $YCrB_4$ and $ThMoB_4$ types are characterized by two-dimensional boron nets with condensed five- and seven-membered rings (Fig. 2a and c), boron atoms in the $ErNiB_4$-type build up a 3D framework (Fig. 2d).

The tendency of $REMB_4$ to form a certain structure correlates with the size of *RE* and *M* atoms [2] and is confirmed also by the examination of a newly reported compound with $ErNiB_4$ structure [30]. Thus, using the atomic radii after Ref. [31], ternary $REMB_4$ compounds with a $r(RE)/r(M)$ ratio of about 1.10–1.43 adopt crystal structure types consisting of planar boron networks, i.e., $YCrB_4$ and $ThMoB_4$. The first type is realized most often for the lanthanides (with $r(RE)/r(M) = 1.21$–1.43) and for some actinides. The $ThMoB_4$ type occurs for thorium and uranium compounds. Nevertheless, the distinction between these structure types solely on the basis of $r(RE)/r(M)$ ratio is not sharp. E.g., the actinide borides with $YCrB_4$-type structure have $r(RE)/r(M)$ ratios between 1.15 and 1.25 and for the compounds with $ThMoB_4$ type this ratio is 1.10–1.33. The $ErNiB_4$ structure type is known solely with a $r(RE)/r(\mathrm{Ni})$ ratio of about 1.42–1.47. Interestingly, for the Er–Ni–B system a ratio of $r(\mathrm{Er})/r(\mathrm{Ni}) = 1.42$ (which is on the lower boundary) is favorable for the formation of compounds with the $YCrB_4$ type as well as with the $ErNiB_4$ type, which was indeed experimentally observed [30]. This case demonstrates that the formation energies of the respective structure modifications for certain $RERhB_4$ compounds are very similar.

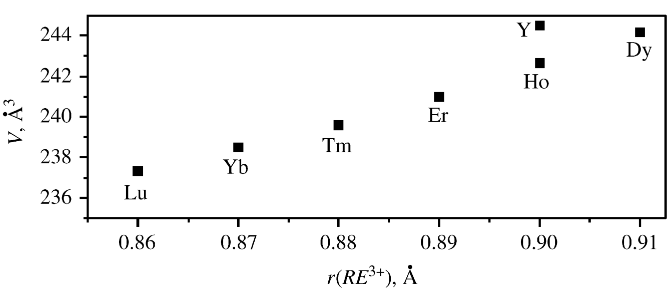

Fig. 1. Unit cell volumes of $RERhB_4$ compounds vs. trivalent cation radii (after [31]).

The closest Rh–Rh interatomic distances of 2.7441(8) Å are slightly longer than interatomic distances of 2.69 Å in *ccp* rhodium [31]. All distances involving rare-earth atoms (e.g., $d(\mathrm{Yb–Yb}) = 3.5172(6)$ Å, $d(\mathrm{Yb–Rh}) = 2.9478(7)$ Å, $d(\mathrm{Yb–B}) = 2.596(7)$ Å in $YbRhB_4$) are significantly shorter than the sum of the corresponding atomic radii ($r(\mathrm{Yb}) = 1.94$ Å, $r(\mathrm{Rh}) = 1.34$ Å, $r(\mathrm{B}) = 0.88$ Å [31]). This indicates a different electronic situation for Yb and other *RE* metals in $RERhB_4$ compared with the elemental metals, which is in agreement with the analysis of the chemical bonding.

The interatomic distances between boron atoms in $RERhB_4$ (Table 6) vary between 1.73 and 1.87 Å. They are comparable with average distances of 1.77 Å in β-boron [31] and are also similar to distances in the recently investigated boron-rich compound $Mg_2Rh_{1-x}B_{6+2x}$, where planar boron nets are formed by pentagonal, hexagonal, and heptagonal rings [32]. The boron–boron distances within the nets vary in the range from 1.68 to 1.83 Å.

3.2. Electron localizability indicator

In order to understand the structural features of the $RERhB_4$ compounds, the analysis of chemical bonding in real space was

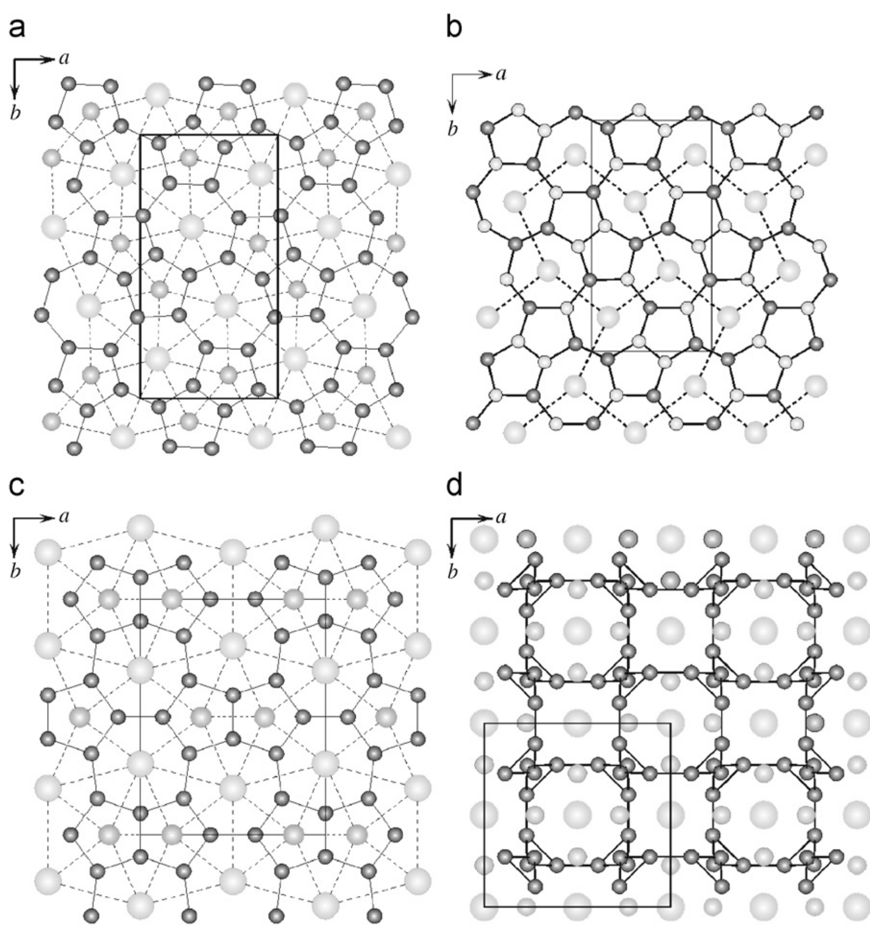

Fig. 2. Planar polyanions and cationic arrangement in the crystal structures of $YCrB_4$ (a), ScC_2B_2 (b), $ThMoB_4$ (c), $ErNiB_4$ (d). *RE* — large white spheres; *M* — small white spheres; B-small dark spheres; C — small white spheres.

Table 5
Crystal structures of the ternary compounds $REMB_4$ (references are given in the fields)

RE	M												
	Al	V	Cr	Mn	Fe	Co	Ni	Mo	Ru	Rh	W	Re	Os
Sc					[55][a]	[55][a]	[55]						
Y		[44][b]	[49][a]	[44][a]	[56][a]	[59][a]	[29][b]	[64][a]	[58][a]	[a,c]	[64][a]	[64][a]	[58][a]
La													
Ce			[50][a]				[29][b]					[52][a]	
Pr			[51][a]	[53][a]			[29][b]						
Nd			[51][a]	[53][a]			[29][b]						
Sm			[51][a]	[54][a]	[57][a]		[29][b]						
Eu													
Gd		[44][a]	[49][a]	[44][a]	[58,59][a]	[59][a]	[29][b]	[64][a]	[58][a]		[64][a]	[64][a]	[58][a]
Tb		[44][a]	[49]	[44][a]	[59][a]	[59][a]	[29][b]	[64][a]	[58][a]		[64][a]	[64][a]	[58][a]
Dy		[44][a]	[49][a]	[44][a]	[59][a]	[59][a]	[29][b]	[64][a]	[58][a]	[d]	[64][a]	[64][a]	[58][a]
Ho	[41][a]	[44][a]	[49][a]	[44][a]	[59][a]	[59][a]	[29][b]	[64][a]	[58][a]	[d]	[64][a]	[64][a]	[58][a]
Er	[41][a]	[44,45][c]	[49][a]	[52][a]	[59][a]	[59][a]	[29,63][d]	[64][a]	[58][a]	[d]	[64][a]	[64][a]	[58][a]
Tm	[42][a]		[49][a]	[52][a]	[59][a]	[59][a]	[63][a]		[58][a]	[d]			[58][a]
Yb	[13,43][f]		[52][a]	[52][a]	[60,61][a]	[60,62][a]	[63][a]		[58][a]	[d]		[52][b]	[58][a]
Lu	[13,43][f]		[49][a]	[52][a]	[59][a]	[59][a]	[63][a]		[66][a]	[d]			[66][a]
Th		[46][e]						[46][e]			[46][e]	[46][e]	
U		[47,48][a]	[47,48][a]	[47][a]	[47,48][a]	[47,48][a]	[29][b]	[47][e]	[66][e]		[47][e]	[47][e]	[66][e]
Pu								[65][a]	[65][f]		[65][a]	[65][a]	[65][f]

[a] Structure type $YCrB_4$.
[b] Structure type $ErNiB_4$.
[c] This work.
[d] Structure types $YCrB_4$ and $ErNiB_4$.
[e] Structure type $ThMoB_4$.
[f] Structure types $YCrB_4$ and $ThMoB_4$.

Table 6
Boron–boron interatomic distances (in Å) and the respective electron counts (n) in the $RERhB_4$ compounds

Atoms	$YRhB_4$		$ErRhB_4$	$TmRhB_4$	$YbRhB_4$	
	d (Å)	*n*(B–B)	*d* (Å)	*d* (Å)	*d* (Å)	*n*(B–B)
B1–B2	1.763(7)	2.39	1.76(1)	1.76(1)	1.76(1)	2.42
B1–B4	1.787(8)	2.35	1.79(1)	1.77(1)	1.76(1)	2.38
B1–B4	1.860(8)	2.81	1.86(1)	1.85(1)	1.87(1)	2.75
B2–B2	1.733(8)	2.59	1.73(1)	1.73(1)	1.72(1)	2.56
B2–B3	1.740(8)	2.46	1.73(1)	1.74(1)	1.73(1)	2.47
B2–B1	1.763(7)	2.39	1.76(1)	1.76(1)	1.76(1)	2.42
B3–B2	1.740(8)	2.46	1.73(1)	1.75(1)	1.73(1)	2.47
B3–B3	1.784(8)	2.31	1.77(1)	1.75(1)	1.75(1)	2.34
B3–B4	1.855(7)	2.75	1.83(1)	1.86(1)	1.85(1)	2.70
B4–B1	1.787(8)	2.35	1.79(1)	1.77(1)	1.76(1)	2.38
B4–B3	1.855(7)	2.70	1.83(1)	1.85(1)	1.87(1)	2.70
B4–B1	1.860(8)	2.81	1.86(1)	1.86(1)	1.85(1)	2.75

performed for $YRhB_4$ and $YbRhB_4$ applying the electron localizability indicator (ELI-D). The questions addressed were, what kind of bonding is responsible for the formation of the boron layers, and what type of atomic interactions can be found between the metals and boron network. Within the planar boron network (Fig. 3a), ELI-D shows maxima (attractors) located in the vicinity of the middle points of the B–B contacts, revealing the two-centre interaction in the boron substructure formed by three-bonded atoms (Fig. 3b). The basins of the B–B maxima interconnect at lower values of ELI-D to one basin set [33] of the boron network. Such topology of ELI-D observed for boron network in $YRhB_4$ and for $YbRhB_4$ is well in agreement with the results obtained for $Mg_2Rh_{1-x}B_{6+2x}$ [32], $TmAlB_4$ [14], $Al_{0.9}B_2$ [34] and $Mg_{0.95}B_2$ [35], where the ELI (ELF) maxima were also found either at the mid-points of the B–B contacts or close to them. In the compounds above, the boron atoms form planar networks with five-, six- and seven-member rings. No distinct ELI (ELF) attractors between the boron nets and the metal species were found in all compounds mentioned, except for $TmAlB_4$ where attractors of ELF were observed between boron and aluminum atoms suggesting here a covalent bonding [14].

Integration of the electron density within the basins of the B–B attractors for $YRhB_4$ yields electron counts between 2.31 and 2.81 electrons per bond for $YRhB_4$ and between 2.34 and 2.75 electrons per bond for $YbRhB_4$ (Table 6), giving in average 2.60 and 2.66 electrons per bond for $YRhB_4$ and for $YbRhB_4$, respectively. Similar electron counts are observed for the $Mg_2Rh_{1-x}B_{6+2x}$ structure (2.4–3.2 electrons per bond), and for the binary borides $Mg_{0.95}B_2$ (2.5 electrons per bond), and for $Al_{0.9}B_2$ (2.67 electrons per bond). Taking in account 2.09 electrons found per boron atom in the first shell in both compounds we obtain in total six electrons per three-bonded boron atom.

Spherical distribution of ELI was found in the first three shells of yttrium and rhodium atoms in $YRhB_4$ (Fig. 3c) and for the first four shells of ytterbium in $YbRhB_4$. The fourth (penultimate) shell for yttrium and rhodium in $YRhB_4$ as well as the penultimate (fifth) shell of ytterbium in $YbRhB_4$ show clear deviations from sphericity (Figs. 3c and d). This is a signature of the participation of the electrons of the penultimate shells in the interaction within the valence region [33]. Integration of the electron density within the four shells gives electron counts of 43.03 for rhodium and 36.82 for yttrium in $YRhB_4$ as well as 68.02 for ytterbium (five shells) and 42.87 for rhodium in $YbRhB_4$, indicating that rhodium, yttrium, and ytterbium participate with roughly two electrons each in the bonding basins within the boron network.

From the consideration above, the space of each crystal structure can be divided into three constituents: basin set of the boron network, basins of the inner shells of rhodium, basins of the inner shells of yttrium or ytterbium. Each of the basin sets has its own population. Taking the electronic population of each basin and subtracting the electron numbers for neutral atoms of this basin one obtains the following balances, which may be called balances of the ELI-based oxidation numbers (ELIBON): $Y^{2.18+}Rh^{1.97+}[B^{0.99-}]_4$, simplified $Y^{2+}Rh^{2+}[B^{1-}]_4$, and

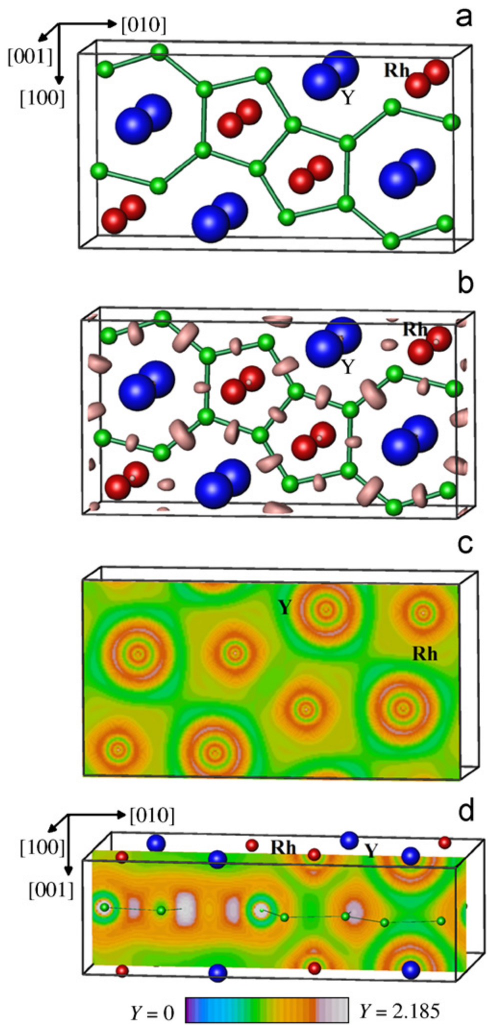

Fig. 3. Electron localizability indicator (ELI-D, Y) in $YRhB_4$: (a) crystal structure view along [001]; (b) isosurface of $Y = 1.73$ visualize positions of ELI-D attractors revealing the two-centre bonding within the boron network; (c) section of ELI-D at $x = 0$; and (d) section of ELI-D through the yttrium and rhodium positions.

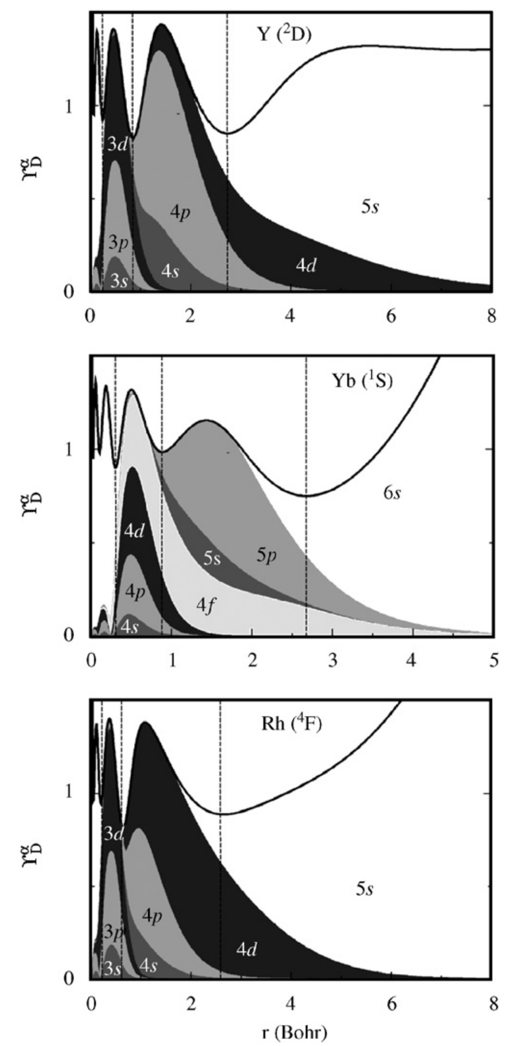

Fig. 4. Electron localizability indicator r_D^α for isolated atoms (majority "α" spin) of Y (configuration ^2D), Yb (^1S) and Rh (^4F).

$Yb^{1.98+}Rh^{2.13+}[B^{1.08-}]_4$, simplified $Yb^{2+}Rh^{2+}[B^{1-}]_4$. Despite the semantical similarity, these balances definitely neither imply primarily any ionic interaction, nor suggest that Rh, Y or Yb participate only with the s electrons in the bonding basins of the boron network.

In order to understand, which electrons are contributed by Rh, Y or Yb to the basin set of the boron network, ELI-D calculations were performed for the isolated atoms (Fig. 4). Application of the orbital charge decomposition of ELI-D formalism [24] clearly reveals the mixed contribution of the 5s and 4d electrons to the last shell of yttrium in ^2D state (0.87 5s+0.32 4d in majority channel) and rhodium in ^4F state (0.76 5s+0.37 4d in majority channel) as well as the 6s, 5p and 4f contributions (0.82 6s+0.08 5p+0.07 4f) to the last shell of ytterbium in ^1S state. This clearly shows the participation of the electrons of the inner shells of metal species in the basin set of the boron network.

3.3. QTAIM

In order to shed more light on the character of interaction between the boron substructure and the metal species in the crystal structures of $YRhB_4$ and $YbRhB_4$ the charges for the atoms QTAIM were calculated by integration of the total electron density within the atomic basins obtained by the topological analysis of the electronic density (Fig. 5). The following charges were calculated: Y — 37.38 e$^-$ ($Y^{1.62+}$), Rh — 45.09 e$^-$ ($Rh^{0.09-}$), B1 — 5.44 e$^-$ ($B^{0.44-}$), B2 — 5.65 e$^-$ ($B^{0.65-}$), B3 — 5.39 e$^-$ ($B^{0.39-}$) and B4 — 5.13 e$^-$ ($B^{0.13-}$) for $YRhB_4$, and Yb — 68.50 e$^-$ ($Yb^{1.50+}$), Rh–45.11 e$^-$ ($Rh^{0.11-}$), B1–5.34 e$^-$ ($B^{0.34-}$), B2–5.53 e$^-$ ($B^{0.53-}$), B3 — 5.36 e$^-$ ($B^{0.36-}$) and B4 — 5.16 e$^-$ ($B^{0.16-}$) for $YbRhB_4$. These results reveal that with QTAIM the charge transfer from the rare-earth species to the boron network is large but definitely smaller than formally expected for RE^{3+} or RE^{2+}. The charge transfer from rhodium to the boron network is around zero, confirming the covalent bonding in this region. This is in agreement with the small electronegativity difference between boron and rhodium. In the topology of ELI, this interaction manifests in the structuring of the penultimate shell but not by the formation of the designated ELI attractor. A merely 'flat' landscape (cf. [36]) of ELI was observed on the Rh–B contacts at the positions where separated attractors are found, e.g., between the according Al and B positions in $TmAlB_4$ [15], in agreement with the previous theoretical investigations [33] and bonding observations for intermetallic rhodium compounds $RhBi_4$ [37], Rh_3Bi_{14}, $RhBi_{12}Br_2$ [38], Rh_4Ga_{21} and Rh_3Ga_{16} [25], where either less pronounced attractors or merely structuring of the penultimate Rh shell were found as fingerprints for the Rh–Bi or Rh–Ga interactions.

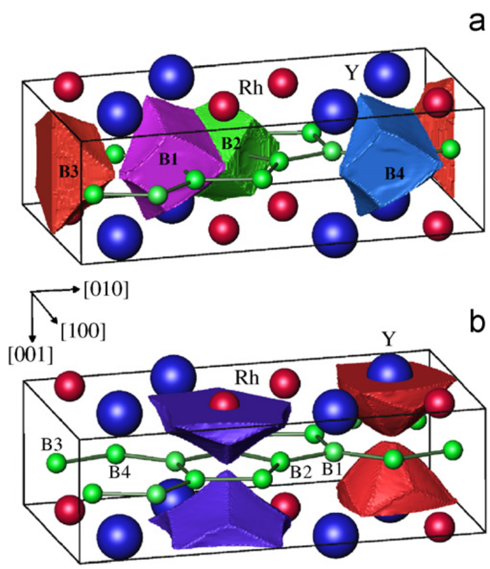

Fig. 5. QTAIM atoms in $YRhB_4$: (a) shapes of boron atoms and (b) shapes of yttrium and rhodium atoms.

Thus $YRhB_4$ and $YbRhB_4$ can be described by a covalently bonded 3-D polyanion containing planar nets of three-bonded boron atoms interconnected by the rhodium atoms with the Y or Yb cations sandwiched in the cavities of the polyanion. Such electronic structure of the polyanionic network seems to be very stable: the boron–boron distances do not vary noticeably for different *RE* components (Table 6). However, there is no correlation between the B–B bond length and the respective electron count (Table 6), similar as was already found for $Mg_2Rh_{1-x}B_{6+2x}$ [32].

3.4. Physical properties

Yb L_{III} X-ray absorption spectrum of $YbRhB_4$ at ambient temperature (Fig. 6) reveals a single-peak picture. The position of the peak (8944 eV) coincides with that of Yb_2O_3, revealing the electronic state $4f^{13}$ for ytterbium.

The temperature dependence of the inverse magnetic susceptibility for $TmRhB_4$ and $YbRhB_4$ is shown in Fig. 7. Although magnetic transitions have been observed previously for $TmAlB_4$ [14,15] and also for $ErAlB_4$ [39], no anomalies indicative for a magnetic transition are observed for either $TmRhB_4$ or $YbRhB_4$ above 1.8 K. The ytterbium compound shows typical behavior for a $^2F_{7/2}$ crystal electric field state (CEF) of the $4f^{13}$ configuration of Yb^{3+} ions (in agreement with the X-ray absorption spectrum). Within the temperature range $200\,K<T<400\,K$ a Curie–Weiss fit yields the parameters $\Theta_P=-30\,K$ and $\mu_{eff}=4.25\mu_B$. χ shows minor changes in the curvature at low temperatures (Fig. 7, inset), but no obvious transitions are observed above 1.8 K.

$TmRhB_4$ shows Curie–Weiss behavior over a wide temperature range and from the Curie–Weiss fit in the temperature range $30\,K<T<400\,K$, the parameters $\Theta=-9.8\,K$ and $\mu_{eff}=7.49\mu_B$ are determined, the latter agreeing well with the value expected for the $^3H_6$ ground multiplet of Tm^{3+} ($4f^{12}$ configuration).

The above results of the analysis of the chemical bonding are not in contradiction to the effective magnetic moments for the *RE* species and the XAS spectrum, because both physical properties indicate the population of the inner shells (4*f* states), which seem not to have sizable influence on the valence region.

The specific heat $C_p(T,H)$ of $TmRhB_4$ and $YbRhB_4$ is plotted in Fig. 8 in a C_P/T vs. T representation. C_P/T of $YbRhB_4$ in zero field shows a strong upturn below 5 K with a peak around 3.5 K

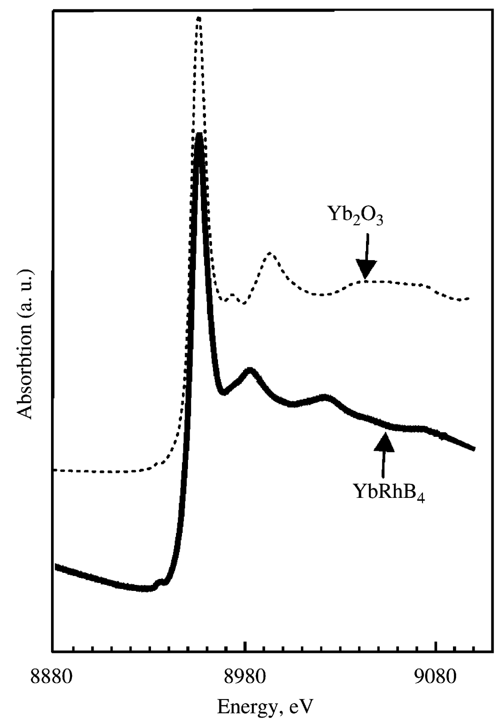

Fig. 6. X-ray absorption spectrum of $YbRhB_4$ in comparison with the reference Yb_2O_3.

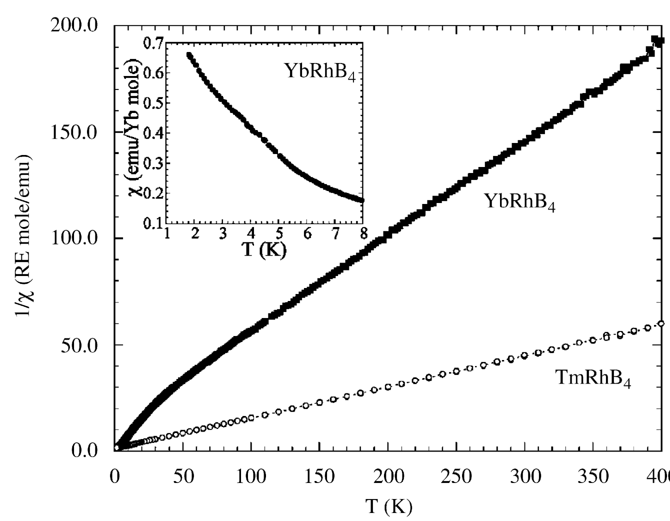

Fig. 7. Temperature dependence of inverse magnetic susceptibility for $TmRhB_4$ (○) and $YbRhB_4$ (■). The inset shows low-temperature susceptibility data for $YbRhB_4$.

indicative for a magnetic transition. At lower temperatures a further sharp peak at 2.3 K is observed. With increasing magnetic fields both anomalies are depressed to lower temperatures indicating an antiferromagnetic character of the transitions. For fields $\mu_0H>4\,T$, a Schottky anomaly appears due to the Zeeman splitting of the CEF ground state. As noted above, significant anomalies are not detected in the magnetic susceptibility of $YbRhB_4$ and therefore the possibility of impurity effects must be considered. However, a careful examination of the crystal measured did not reveal the presence of impurities in substantial quantities which would be necessary to account for the large change in C_P below 5 K if it would be due to impurity effects. Therefore, it is indicated that an intrinsic antiferromagnetic transition occurs in $YbRhB_4$ at 3.5 K. The sharp narrow peak at

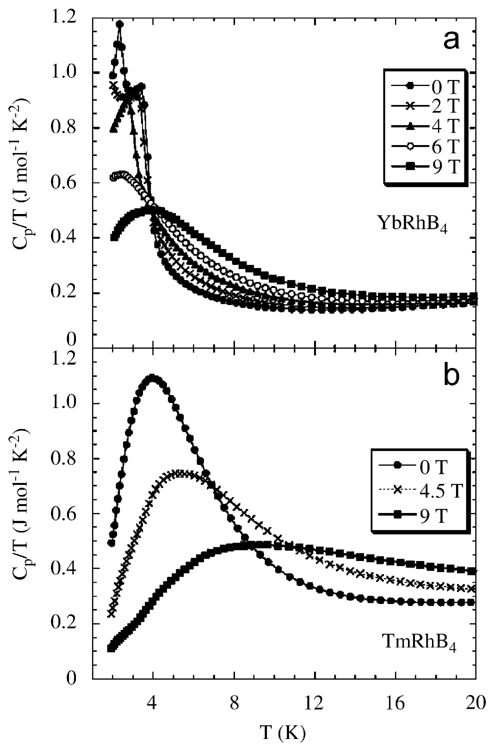

Fig. 8. Specific heat of $YbRhB_4$ (a) and $TmRhB_4$ (b) vs. temperature in different magnetic fields.

2.3 K may indicate a further transition. However, this temperature coincides with the commonly observed impurity Yb_2O_3 [40] and is not straightforward understandable accounting only one Yb position in the crystal structure. Thus, the second transition cannot be concluded decisively. An estimate of the magnetic and CEF contribution related to the 4*f* electrons is difficult due to the lack of a non-magnetic reference sample. Taking the zero-field specific heat at 20 K as a maximum estimate for the lattice heat capacity, a minimum Debye temperature of 300 K can be calculated for the low-temperature region. Subtraction of the lattice contributions and calculation of the entropy $S_{4f}(T)$ results in values around $R\ln 2$ at 20 K for high magnetic fields (for low fields part of the entropy is released only well below the minimum measured temperature), confirming an isolated Kramers doublet ground state of the $^2F_{7/2}$ multiplet.

No magnetic transitions are indicated by the C_P data for $TmRhB_4$. A large Schottky anomaly is observed with a maximum at 4 K for zero field. Taking the same lattice background as previously assumed, a magnetic entropy $S_{4f}(T)$ is obtained which increases to values beyond $R\ln 2$ and almost reaches $R\ln 3$ at 20 K, indicating the presence of three states of the 13-fold degenerate $^3H_6$ multiplet within 20 K. A fit of the zero-field Schottky anomaly reveals a level scheme with the lowest singlets at 0, 11, and $\approx$24 K. With increasing field this Schottky anomaly broadens and shifts toward higher temperatures. Magnetic order cannot be expected for such a CEF scheme, in contrast to the Kramers doublet ground state in the Yb compound.

4. Conclusions

The compounds *RE*RhB_4 (*RE* = Y, Dy, Ho, Er, Tm, Yb, Lu) were synthesized. They crystallize with the $YCrB_4$ type. Analysis of chemical bonding with quantum chemical tools in real space (electron localizability indicator, QTAIM atoms) for $YRhB_4$ and $YbRhB_4$ reveals covalent bonding within the planar boron nets interconnected by rhodium to the 3-D polyanion. The charge transfer (calculated for QTAIM atoms) from the *RE* species to the boron part of the polyanion is quite pronounced indicating predominantly ionic interaction. The $4f^{13}$ state of ytterbium in $YbRhB_4$ is established by XAS and magnetic susceptibility measurements. A Schottky feature in specific heat is found in $TmRhB_4$ at low temperatures indicating crystal electric field splitting of the Tm 4*f* state and a singlet ground state. The ytterbium compound shows an antiferromagnetic transition at 3.5 K and a possible further transition at 2.3 K.

Acknowledgments

Authors thank U. Burkhardt, S. Budnyk and E. Welter (of HASYLAB, DESY, Hamburg) for the XAS measurements and acknowledge F.R. Wagner for valuable discussions.

References

[1] Yu.B. Kuzma, N.F. Chaban, Binary and Ternary Systems containing Boron, Metallurgia, Moscow, 1990.
[2] Yu.B. Kuzma, Crystal Chemistry of Borides, Vyscha Shkola, Lviv, 1983.
[3] N.F. Chaban, S.I. Mykhalenko, Yu.B. Kuzma, Neorg. Mater. 32 (1996) 44.
[4] N.F. Chaban, S.I. Mykhalenko, Yu.B. Kuzma, Poroshk. Metall. 11/12 (1998) 75.
[5] P. Villars, L.D. Calvert, Pearson's Handbook of Crystallographic Data for Intermetallic Phases, Materials Park, OH, 1996.
[6] P. Rogl, in: J.J. Zuckermann, A.P. Hagen (Eds.), Inorganic Reactions and Methods, vol. 13, Wiley, New York, 1991, p. 85.
[7] P. Rogl, In: K.A. Gschmeidner Jr., L. Eying (Eds.), Handbook on the Physics and Chemistry of Rare Earths, vol. 6, 1984, pp. 335.
[8] T. Ohtani, B. Chevalier, P. Lejay, J. Etourneau, M. Vlasse, P. Hagenmuller, J. Appl. Phys. 54 (1983) 5928.
[9] D.C. Johnston, Solid State Commun. 24 (1977) 669.
[10] K.H.J. Buschow, in: V.I. Matkovich (Ed.), Boron and Refractory Borides, Heidelberg, Berlin, 1977, p. 494.
[11] T. Mori, Higher borides, in: K.A. Gschneidner Jr., J.-C. Bünzli, V. Pecharsky (Eds.), Handbook on the Physics and Chemistry of Rare-earths, vol. 38, North-Holland, Amsterdam, chapter 238, p. 105–173.
[12] S. Okada, T. Shishido, T. Mori, K. Kudou, K. Iizumi, T. Lundström, K. Nakajima, J. Alloys Compd. 408–412 (2006) 547.
[13] R.T. Makaluso, S. Nakatsukuji, K. Kuga, E.L. Thomas, Y. Machida, Y. Maeno, Z. Fisk, J.Y. Chan, Chem. Mater. 19 (2007) 1918.
[14] T. Mori, H. Borrmann, S. Okada, K. Kudou, A. Leithe-Jasper, U. Burkhardt, Yu. Grin, Phys. Rev. B 76 (2007) 064404.
[15] T. Mori, S. Okada, K. Kudou, J. Appl. Phys. 97 (2005) 10A910.
[16] WinXPow (version 2.08). STOE and Cie GmbH, Darmstadt, 2003.
[17] L.G. Akselrud, P.Yu. Zavalii, Yu. Grin, V.K. Pecharsky, B. Baumgartner, E. Wölfel, Mater. Sci. Forum 133–136 (1993) 335.
[18] U. von Barth, L. Hedin, J. Phys. C 5 (1972) 1629.
[19] O. Jepsen, A. Burkhardt, O.K. Andersen, The Program TB-LMTO-ASA, Version 4.7, Max-Planck-Institut für Festkörperforschung, Stuttgart, 1999.
[20] O.K. Andersen, Phys. Rev. B 12 (1975) 3060.
[21] M. Kohout, Int. J. Quantum Chem. 97 (2004) 651.
[22] M. Kohout, Basin, Version 4.2, 2007.
[23] R.F.W. Bader, Atoms in Molecules: A Quantum Theory, Oxford University Press, Oxford, 1999.
[24] F.R. Wagner, V. Bezugly, M. Kohout, Yu. Grin, Chem. Eur. J. 13 (2007) 5724.
[25] E. Clementi, C. Roetti, Atom. Data Nucl. Data Tables 14 (1974) 218.
[26] ADF 2007.01, SCM, Vrije Universiteit Amsterdam, The Netherlands.
[27] C.S. Smith, Q. Johnston, P.C. Nordine, Acta Crystallogr. 19 (1965) 668.
[28] P. Rogl, H. Nowotny, Monatsh. Chem. 205 (1974) 1082.
[29] Yu.B. Kuzma, N.S. Bilonizhko, V.K. Pecharsky, L.G. Akselrud, Sov. Phys. Crystallogr. 29 (1984) 259.
[30] N.F. Chaban, I.V. Veremchuk, Yu.B. Kuzma, J. Alloys Compd. 370 (2004) 129.
[31] J. Emsley, The Elements, Oxford University Press, Oxford, 1998.
[32] A.M. Alekseeva, A.M. Abakumov, P.S. Chizhov, A. Leithe-Jasper, W. Schnelle, Yu. Prots, J. Hadermann, E.V. Antipov, Yu. Grin, Inorg. Chem. 46 (2007) 7378.
[33] M. Kohout, F.R. Wagner, Yu. Grin, Theor. Chem. Acc. 108 (2002) 150.
[34] U. Burkhardt, V. Gurin, F. Haarmann, H. Borrmann, W. Schnelle, A. Yaresko, Yu. Grin, J. Solid State Chem. 177 (2004) 389.
[35] J. Schmidt, W. Schnelle, Yu. Grin, R. Kniep, Solid State Sci. 5 (2003) 535.
[36] Yu. Grin, F.R. Wagner, M. Armbrüster, M. Kohout, A. Leithe-Jasper, U. Schwarz, U. Wedig, H.G. von Schnering, J. Solid State Chem. 179 (2006) 1707.
[37] Yu. Grin, U. Wedig, H.G. von Schnering, Angew. Chem. 107 (1995) 1318; Yu. Grin, U. Wedig, H.G. von Schnering, Angew. Chem. Int. Ed. 34 (1995) 1204.
[38] M. Boström, Yu. Prots, Yu. Grin, J. Solid State Chem. 179 (2006) 2472.
[39] T. Mori, R. Cardoso-Gil, A. Leithe-Jasper, W. Schnelle, H. Borrmann, Yu. Grin, J. Appl. Phys. 103 (2008) 073730.

[40] J.P.S. Klasse, J.W.E. Sterkenburg, A.H.M. Bleyendaal, F.R. de Boer, Solid State Commun. 12 (1973) 561;
H. Bonrath, K.H. Hellwege, K. Nicolay, G. Weber, J. Phys.: Condens. Matter 4 (1966) 382.
[41] S.I. Mikhalenko, N.F. Chaban, Yu.B. Kuzma, Powder Metall. Met. Ceram. 33 (1994) 584.
[42] S. Okada, K. Kudou, Y. Yu, T. Lundström, Jpn. J. Appl. Phys. 33 (1994) 2663.
[43] S.I. Mikhalenko, Yu.B. Kuzma, M.M. Korsukova, V.N. Gurin, Neorg. Mater. 16 (1980) 1325.
[44] Yu.B. Kuzma, Dopov. Akad. Nauk Ukr. RSR Ser. A 8 (1970) 756.
[45] N. Chaban, Yu. Prots, Yu.B. Kuzma, Yu. Grin, Z. Kristallogr, New Crystal. Struct. 217 (2002) 315.
[46] P. Rogl, H. Nowotny, Monatsh. Chem. 105 (1974) 1082.
[47] P. Rogl, H. Nowotny, Monatsh. Chem. 106 (1975) 381.
[48] I.P. Valyovka, Yu.B. Kuzma, Dopov. Akad. Nauk Ukr. RSR A 7 (1975) 652.
[49] Yu.B. Kuzma, Sov. Phys. Crystallogr. 15 (1970) 312.
[50] Yu.B. Kuzma, S.I. Svarichevskaya, V.N. Fomenko, Neorg. Mater. 9 (1973) 1372.
[51] S.I. Mikhalenko, Yu.B. Kuzma, Dopov. Akad. Nauk Ukr. RSR A 39 (1977) 951.
[52] N.F. Chaban, S.I. Mikhalenko, Yu.B. Kuzma, Neorg. Mater. 32 (1996) 36.
[53] S.I. Mikhalenko, Yu.B. Kuzma, T.D. Chuchman, Neorg. Mater. 26 (1990) 1968.
[54] S.I. Mikhalenko, Yu.B. Kuzma, Neorg. Mater. 27 (1991) 1793.
[55] L.V. Zavalii, Yu.B. Kuzma, S.I. Mikhalenko, Neorg. Mater. 24 (1988) 1814.
[56] D. Givord, P. Tenaud, J.M. Moreau, J. Less-Common Met. 123 (1986) 109.
[57] H.F. Braun, K. Yvon, Acta Crystallogr. B 36 (1980) 2400.
[58] R. Sosczak, P. Rogl, J. Solid State Chem. 27 (1979) 343.
[59] G.F. Stepanchikova, Yu.B. Kuzma, Vestn. Lvov. Univ. 19 (1977) 37.
[60] O.M. Dub, N.F. Chaban, Yu.B. Kuzma, Neorg. Mater. 21 (1985) 1718.
[61] I.V. Veremchuk, N.F. Chaban, V.S. Babizhetskyy, O.T. Pilyushchak, Yu.B. Kuzma, Neorg. Mater. 41 (2005) 700.
[62] I.V. Veremchuk, N.F. Chaban, V.N. Davydov, Yu.B. Kuzma, Neorg. Mater. 40 (2004) 1301.
[63] N.F. Chaban, G.V. Chernyak, Yu.B. Kuzma, Neorg. Mater. 17 (1981) 1120.
[64] Yu.B. Kuzma, L.M. Svarichevska, Dopov. Akad. Nauk Ukr. RSR Ser. A 32 (1972) 166.
[65] P. Rogl, P.E. Potter, H.R. Haines, J. Nucl. Mater. 160 (1988) 107.
[66] P. Rogl, L. Delong, J. Less-Common Met. 91 (1983) 97.